Carrier kinetics in a surface-excited semiconductor slab: Influence of boundary conditions

T. Kuhn and G. Mahler
Institut für Theoretische Physik I, Universität Stuttgart, Pfaffenwaldring 57, 7000 Stuttgart 80, Federal Republic of Germany
(Received 4 August 1986)

The stationary Boltzmann equation is solved for electron-hole pairs injected in the semiconductor surface region by means of a monochromatic light field. Profiles of hydrodynamic variables are given as a function of excitation conditions and surface properties. In general, the respective currents result not only from spatial inhomogeneities, but also from ballistic or drift contributions, which can be traced back to the kinetic boundary conditions. Numerical results are given for material parameters typical of indirect semiconductors like Si.

I. INTRODUCTION

Kinetic theories for space-dependent phenomena with boundaries have applications in many fields of physics, e.g., classical gas dynamics,[1] plasma physics,[2] neutron transport processes,[3] and solid state physics. In semiconductor physics they are important both for device modeling and for a fundamental understanding of transport phenomena.

Transport processes of optically generated electron-hole plasmas (EHP's) in semiconductors have been the object of many investigations during the last years. Experiments have been carried out under nonstationary conditions, e.g., time-of-flight measurements,[4] optical imaging,[5] light scattering,[6] and expansion to Mott transition,[7] as well as under stationary conditions, e.g., luminescence line shape,[8] gain measurements,[9] and Raman scattering.[10] Interpretation of the experimental data in terms of a simple diffusion equation failed as a result of unexpectedly large experimental plasma velocities. Wolfe and co-workers[5,11,12] favored a phonon wind as driving force for the EHP as originally proposed by Bagaev *et al.*[13] Mahler[14,15] introduced a thermodiffusion model, which takes into account not only density gradients, but also temperature gradients, and postulated the possibility of an additional drift term, caused by surface effects. However, a severe problem in all hydrodynamic calculations are the appropriate boundary conditions for the various densities and currents: This is so, because in a hydrodynamic description the basic processes, such as acceleration, scattering, generation, and recombination of particles, appear only averaged over all particles. In a kinetic theory, on the other hand, the boundary conditions are closely related to these microscopic processes, in particular to reflection and surface recombination.

The starting point of nearly all semiclassical kinetic theories is the Boltzmann transport equation. In only a few cases an analytical solution of this equation is possible,[16] so various techniques have been developed to get either analytical approximations or numerical solutions. Analytic techniques expand the distribution function in a suitable set of functions,[1] or they assume an *a priori* form of the distribution function that contains parameters.[17] For numerical investigations mainly two methods are used nowadays, the Monte Carlo method,[18] and the iterative technique.[19,20] The latter we use in this paper, because in this case the boundary conditions can easily be incorporated.

II. TRANSPORT MODEL

A complete theory of transport phenomena in semiconductors involves several components—electrons, holes, and the different phonon modes—which are all coupled. In order to make the problem tractable for computation, its description must be reduced to the most relevant features. In a first approximation it is justified to treat the phonon system as a heat bath, i.e., to neglect its deviation from equilibrium due to the interactions with the other components. The remaining two components, electrons and holes, are strongly coupled via electrostatic forces resulting from local charge imbalance. In hydrodynamic theories the assumption of local charge neutrality leads in the "ambipolar transport model" effectively to a single-component description. In kinetic theories this approximation has no simple correspondence, since in a real semiconductor there are different distribution functions even in equilibrium as a result of the different masses and relaxation times of electrons and holes. To avoid this difficulty we take a model semiconductor with equal masses and relaxation times. In this case the kinetic equations of electrons and holes are the same in the absence of an applied electric field and the local charge density remains zero. So we have also kinetically a one-component system, in which the charge shows up as a "pseudospin," decoupled from the kinetic degrees of freedom.

The stationary Boltzmann transport equation (BTE) for this one-component electronic system without external forces is

$$\frac{\hbar\mathbf{k}}{m^*}\nabla_r f(\mathbf{k},\mathbf{r}) = g(\mathbf{k},\mathbf{r}) + \left[\frac{\partial f}{\partial t}\right]_s , \tag{1}$$

where $g(\mathbf{k},\mathbf{r})$ is a generation rate due to the laser light and $(\partial f/\partial t)_s$ is the rate of change of the distribution function

due to scattering and recombination. The geometrical set-up for our system is a semiconductor slab of thickness L in z direction and infinite in x and y direction. The surface at $z=0$ is irradiated by the laser light, which is absorbed in a layer of the penetration depth $1/\lambda$ generating electron-hole pairs. The radial dependence of the laser beam is neglected, which is a good approximation as long as the diameter of the beam is large compared to L. Under this condition the BTE (1) depends only on one spatial coordinate z. Using the concept of self-scattering,[18,19] we add a term $\Gamma f(\mathbf{k},z)$ on both sides of (1). Originally, self-scattering was introduced purely as a mathematical device to get a simpler form of the integral equation, but it can be shown that the iterative procedure is equivalent to the solution of the time-dependent BTE in time steps $\Delta t=1/\Gamma$. We can then integrate (1) treating the right-hand side as an inhomogeneity to get the formal solution

$$f(\mathbf{k},z)=f(\mathbf{k},0)e^{-\gamma z}+\frac{m^*}{\hbar k_z}\int_0^z e^{-\gamma(z-z')}\left[g(\mathbf{k},z')+\left[\frac{\partial f}{\partial t}\right]_s+\Gamma f(\mathbf{k},z')\right]dz' , \tag{2}$$

with

$$\gamma=\frac{m^*\Gamma}{\hbar k_z} .$$

Unique solutions require boundary conditions for the distribution function. We assume that a particle arriving at the surface $z=0$ or $z=L$ is specularly reflected with probability R_0 or R_L and recombines with the corresponding probability $1-R_0$ or $1-R_L$, respectively. The resulting integral equation has different forms for $k_z>0$ and $k_z<0$, so in the following we take throughout $k_z>0$ and introduce the vectors $\mathbf{k}_+=(k_x,k_y,k_z)$ and $\mathbf{k}_-=(k_x,k_y,-k_z)$. We obtain the two equations

$$\begin{aligned} f(\mathbf{k}_+,z)=\alpha(k_z)\Big[&\int_0^z e^{-\gamma z'}S(\mathbf{k}_+,z-z')dz'+R_0e^{-\gamma z}\int_0^L e^{-\gamma z'}S(\mathbf{k}_-,z')dz' \\ &+R_0R_Le^{-\gamma(L+z)}\int_0^{L-z}e^{-\gamma z'}S(\mathbf{k}_+,L-z')dz'\Big] , \end{aligned} \tag{3a}$$

$$\begin{aligned} f(\mathbf{k}_-,z)=\alpha(k_z)\Big[&\int_0^{L-z}e^{-\gamma z'}S(\mathbf{k}_-,z+z')dz'+R_Le^{-\gamma(L-z)}\int_0^L e^{-\gamma z'}S(\mathbf{k}_+,L-z')dz' \\ &+R_0R_Le^{-\gamma(2L-z)}\int_0^z e^{-\gamma z'}S(\mathbf{k}_-,z')dz'\Big] . \end{aligned} \tag{3b}$$

Here we have used the abbreviations

$$\alpha(k_z)=m^*/[\hbar k_z(1-R_0R_Le^{-2\gamma L})] ,$$

$$S(\mathbf{k},z)=g(\mathbf{k},z)+\left[\frac{\partial f}{\partial t}\right]_s+\Gamma f(\mathbf{k},z) .$$

In the following we neglect terms with the product R_0R_L, because they all contain a factor $e^{-\gamma L}$, which is negligible for typical self-scattering rates Γ. The laser with energy $\hbar\omega_L$ creates electron-hole pairs at a fixed excess energy $E_{\text{exc}}=\hbar^2k_L^2/2m^*=\frac{1}{2}(\hbar\omega_L-E_g)$ and isotropic in k space, so we take for the generation rate

$$g(\mathbf{k},z)=g_0\delta(k_L^2-k^2)e^{-\lambda z} . \tag{4}$$

Limiting our calculations to excess energies less than the optical phonon energy $\hbar\omega_{\text{LO}}$ and to temperatures less than $\hbar\omega_{\text{LO}}/k_B$ we can neglect optical phonon scattering. The scattering rate in (1) is modeled by the relaxation-time approximation

$$\left[\frac{\partial f}{\partial t}\right]_s=-\frac{f-f_0}{\tau(k)} , \tag{5}$$

with the relaxation time $\tau(k)$ for acoustic deformation potential scattering

$$\frac{1}{\tau(k)}=\frac{m^*k_BT_LE_1^2}{\pi\hbar^3v_s^2\rho}k \tag{6}$$

and the Maxwell distribution function for a nondegenerate system

$$f_0(\mathbf{k},z)=n'(z)\left[\frac{\hbar^2}{2\pi m^*k_BT_L}\right]^{3/2}\exp\left[-\frac{\hbar^2k^2}{2m^*k_BT_L}\right] .$$

$n'(z)$ is adjusted to satisfy the current continuity equation, T_L is the lattice temperature, E_1 the acoustic deformation potential, ρ the mass density, and v_s the second velocity. To study the influence of electron-electron scattering we add a second scattering rate

$$\left[\frac{\partial f}{\partial t}\right]_e=-\frac{f-f_{0e}}{\tau_e} , \tag{7}$$

with

$$f_{0e}(\mathbf{k},z)=n(z)\left[\frac{\hbar^2}{2\pi m^*k_BT_e(z)}\right]^{3/2}\times\exp\left[-\frac{\hbar^2[\mathbf{k}-\mathbf{k}_e(z)]^2}{2m^*k_BT_e(z)}\right] ,$$

$$n(z)=\int d^3k\,f(\mathbf{k},z) ,$$

$$n(z)\mathbf{k}_e(z)=\int d^3k\,\mathbf{k}f(\mathbf{k},z) ,$$

$$\tfrac{3}{2}n(z)k_BT_e(z)=\frac{\hbar^2}{2m^*}\int d^3k[\mathbf{k}-\mathbf{k}_e(z)]^2f(\mathbf{k},z) .$$

We take a constant scattering time τ_e. This is a rather crude simplification, since the true electron-electron scattering time depends on the wave vector $\mathbf{k}$ as well as on the distribution function itself, but it still represents the main properties of electron-electron scattering: the distribution function tends towards a heated and displaced Maxwellian with temperature T_e and displacement vector $\mathbf{k}_e(z)$ and it satisfies energy and momentum conservation.

According to the symmetry of our problem the distribution function depends only on three arguments, z, k_z, and $k_{||}=(k_x^2+k_y^2)^{1/2}$. We take the $k_{||}$ dependence of $f(\mathbf{k},z)$ to be approximately Maxwellian and integrate (3) over k_x and k_y leading to an integral equation for the one-dimensional distribution function f_1,

$$f_1(k_z,z)=\int dk_x dk_y f(\mathbf{k},z) .$$

The corresponding generation rate is

$$g_1(k_z,z)=\int dk_x\, dk_y\, g(\mathbf{k},z)$$
$$=g_0'\Theta(k_L^2-k_z^2)e^{-\lambda z} , \tag{8}$$

where $\Theta(x)$ denotes the unit step function, i.e., $\Theta(x)=1$ for $x>0$ and $\Theta(x)=0$ for $x<0$. The electron-phonon scattering rate (6) is thus transformed to

$$\tau_1^{-1}(k_z)=\frac{\hbar^2}{m^* k_B T_e}\int_0^\infty k_{||}dk_{||}\tau^{-1}(k_{||},k_z)\exp\left[-\frac{\hbar^2 k_{||}^2}{2m^* k_B T_e}\right]$$
$$=\frac{\sqrt{2}k_B T_L E_1^2 (m^*)^{3/2}(k_B T_e)^{1/2}}{\pi\hbar^4 v_s^2\rho}\left[q+\frac{\sqrt{\pi}}{2}e^{q^2}[1-\Phi(q)]\right] \tag{9}$$

with $q=\hbar|k_z|/(2m^* k_B T_e)^{1/2}$. $\Phi(x)$ is the error function. We use the material parameters $m^*=0.43m_0$, $E_1=8.8$ eV, $\rho=2.33$ g/cm^3, $L=20$ μm, $v_s=9\times10^5$ cm/s, $\tau_e=10$ ps, and $1/\lambda=1$ μm. The values of m^* and E_1 are chosen to reproduce the correct ambipolar diffusion constant for Si, that is, they satisfy

$$(m^*)^{5/2}E_1^2=\tfrac{1}{2}(m_e^{5/2}E_{1e}^2+m_h^{5/2}E_{1h}^2) . \tag{10}$$

Because in the nondegenerate case the BTE is linear with respect to the density, the distribution function is proportional to the laser intensity g_0. So the absolute value of the density is not important and we normalize all density profiles to their respective maximum. To assure numerical stability the self-scattering rate Γ must satisfy

$$\Gamma\geq\frac{1}{\tau_1(k_z)}+\frac{1}{\tau_e}$$

in that region of k_z space, where f_1 is essentially nonzero. We neglect bulk recombination, because in an indirect semiconductor like Si the recombination time is of the order of 1 μs, so in the small samples of 20-μm length surface recombination is the dominant process.

III. RESULTS AND DISCUSSION

A. Influence of the surface model

It is well known that surfaces play an important role in the transport process of carriers. Figure 1 shows the density profiles for three different surface models. In our calculations the surfaces are modeled by reflection coefficients. We take the same reflection coefficient $R=R_0=R_L$ on both sides of the sample. Usually, the effect of a surface is taken into account by a surface-recombination velocity s,[21] which is the normal component of the average velocity of the carriers at the surface. Since this average depends on the shape of the distribution function, there is no simple quantitative connection between those two types of descriptions. Qualitatively it is clear that a small reflection coefficient belongs to a "bad" surface with high s, while a reflection coefficient of unity belongs to a perfect surface without surface recombination. For Si the values for s reported in the literature[21] vary from 10^2 up to some 10^6 cm/s depending on the surface preparation. Figure 2 shows the calculated surface-recombination velocity as a function of the reflection coefficient for two different temperatures. They agree with the experimental range, confirming that values of 10^2 cm/s are very good surfaces, where nearly all carriers are reflected into the sample and only a small fraction recombines via surface states.

B. Reverse diffusion

In previous papers[8,14,15,22] Mahler *et al.* studied the transport of an EHP in a thermodiffusion model. They predicted the possibility of "reverse diffusion," in which the particle current has the same direction as the density gradient. Qualitatively, the origin of this effect is a large

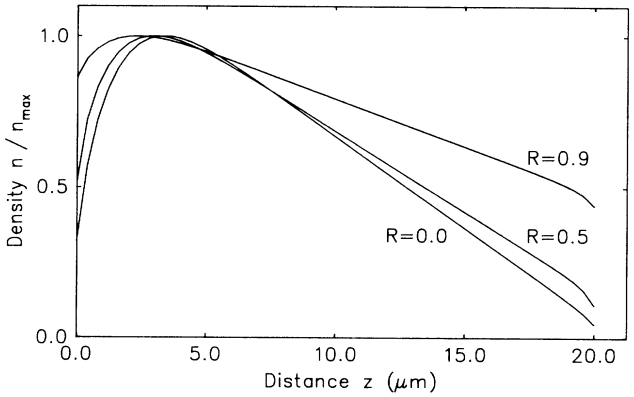

FIG. 1. Density profiles for various reflection coefficients at $T_L=10$ K and $E_{exc}=8$ meV.

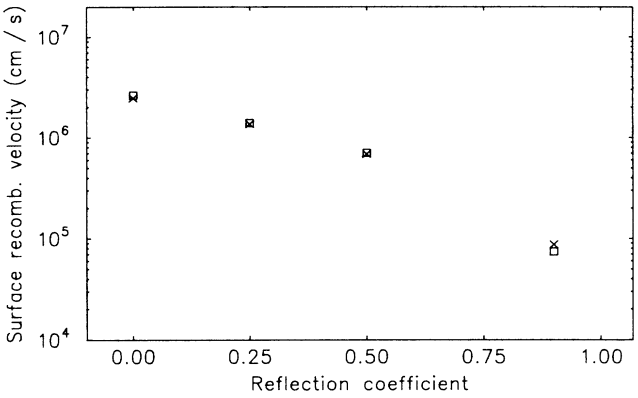

FIG. 2. Surface recombination velocity as a function of reflection coefficient for $E_{exc}=8$ meV. The crosses are calculated for $T_L=10$ K and the squares for $T_L=4$ K.

temperature gradient leading to a strong heat current, which, by means of the thermodiffusion coefficient, in turn implies a strong particle current. If this current becomes too large with respect to the generation rate, a positive density gradient must build up to limit the particle current. Since the ratio between heat and particle current is determined by the excess energy of the laser, this parameter should influence reverse diffusion. Figure 3(a) shows the density profile and Fig. 3(b) the temperature profile for different excess energies. The crosses in Fig. 3(a) mark the points, where the corresponding particle current densities go through zero, so the region between the cross and the density maximum of each curve exhibits reverse diffusion. The width of this region increases with increasing excess energy.

Figure 4(a) and 4(b) show the density and temperature profiles for varying lattice temperature. Again, the crosses mark the points where the particle current density goes through zero. In this case, the region of reverse diffusion increases with decreasing temperature, since for constant excess energy a lower lattice temperature leads to a stronger temperature gradient. Remarkably, the maximum of the density can occur quite far away from the surface. In the 4-K case it is at $z=7$ μm, while generation takes place for $z<1$ μm. The dashed line in Fig. 4(a) demonstrates that reverse diffusion is not an effect of the surface recombination, since this curve is calculated for a perfect surface at $z=0$ ($R_0=1$, $R_L=0$). Of course, in this case the current density is zero at the surface and positive everywhere inside the sample.

C. Time scales

The different relaxation times of the scattering mechanism lead to different transport types according to the time scale on which the process occurs. In a not-too-small sample the usual process is a diffusive motion due to the interaction with the lattice. Except in presence of an external force, this is the dominant type on all time scales long compared to the electron-phonon relaxation time, because this interaction leads to a relaxation of momentum. Only spatial gradients of density or temperature can then be the origin of a carrier motion. When the time scale becomes shorter than the momentum relaxation time, electron-electron interaction becomes the dominant scattering mechanism. Neglecting Umklapp processes, which is in most cases a valid approximation in semiconductors, this interaction is momentum conserving. This means, that if the carrier distribution has an initial drift, this drift is maintained over the entire sample. The *total* momentum of all carriers is conserved. The carrier system behaves quite similar to a liquid, described by the Navier-Stokes equation rather than by a diffusion equation, and a motion is possible although there is no spatial gradient or driving force. Finally, on the shortest time scale, when all scattering processes can be neglected, *each individual* momentum of a carrier is conserved. Then we have ballistic transport, or, as it is called in other fields of solid state physics, coherent transport. In both momentum-conserving cases the main problem is concerned with the origin of the initial net drift of the system. One possibility is the injection of carriers at a surface or an interface, as it occurs in many semiconductor devices.[23] However, in the optical generation no k direction is preferred *a priori*. But the surface can act as a momentum source, since an incoming pair with velocity

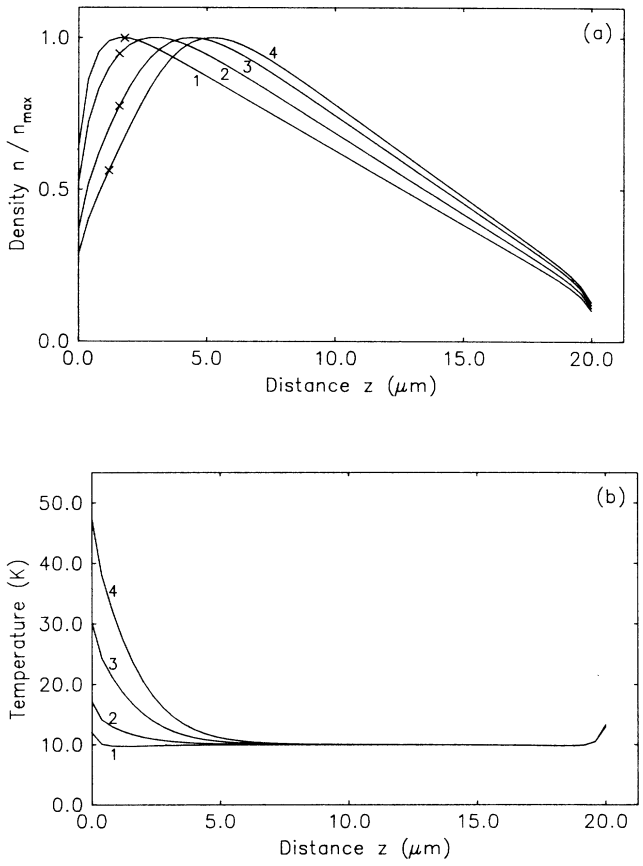

FIG. 3. (a) Density and (b) temperature profiles at $T_L=10$ K and $R=0.5$ for excess energies (1) 2 meV, (2) 8 meV, (3) 28 meV, (4) 60 meV. The crosses in (a) mark the points, where the corresponding current density is zero, so the region between the cross and the maximum of each curve exhibits reverse diffusion.

$v_z<0$ either recombines or is reflected and so transformed into a pair with $v_z>0$, both processes leading to a net drift of the distribution function.

D. Ballistic limit

In the totally ballistic case, i.e., no scattering rate in the BTE, a stationary state cannot exist with the generation rate (8): Integrating Eq. (1) with $(\partial f/\partial t)_s=0$ and

$$g(\mathbf{k},z)=g_0(\mathbf{k})e^{-\lambda z}$$

gives

$$f(\mathbf{k}_+,z)=\frac{m^*}{\hbar k_z\lambda}[(1-e^{-\lambda z})g_0(\mathbf{k}_+)+R_0A(\mathbf{k})]\ , \tag{11a}$$

$$f(\mathbf{k}_-,z)=\frac{m^*}{\hbar k_z\lambda}[-(1-e^{-\lambda z})g_0(\mathbf{k}_-)+A(\mathbf{k})]\ , \tag{11b}$$

with

$$A(\mathbf{k})=\frac{1}{1-R_0R_L}(1-e^{-\lambda L})[g_0(\mathbf{k}_-)+R_Lg_0(\mathbf{k}_+)]\ .$$

If $g_0(k_z=0)\neq 0$, there is a singularity in (11) at $k_z=0$. Physically this is obvious, since carriers with zero velocity stay where they are generated and cannot leave the system (unless we include recombination). For a symmetrical generation rate, $g_0(\mathbf{k}_+)=g_0(\mathbf{k}_-)$, we get, with

$$g_1(k_z)=\int dk_x\,dk_y g(\mathbf{k})\ ,$$

$$G_0=\int_0^\infty dk_z\frac{m^*}{\hbar k_z\lambda}g_1(k_z),\quad G_1=\int_0^\infty dk_z\frac{1}{\lambda}g_1(k_z)\ ,$$

the density

$$n(z)=\int dk_xdk_y\int_0^\infty dk_z[f(\mathbf{k}_+,z)+f(\mathbf{k}_-,z)]$$
$$=G_0\frac{(1+R_0)(1+R_L)}{1-R_0R_L} \tag{12}$$

and current density

$$j(z)=\int dk_x\,dk_y\int_0^\infty dk_z\frac{\hbar k_z}{m^*}[f(\mathbf{k}_+,z)-f(\mathbf{k}_-,z)]$$
$$=G_1\left[2(1-e^{-\lambda z})-(1-e^{-\lambda L})\frac{(1-R_0)(1+R_L)}{1-R_0R_L}\right]. \tag{13}$$

E. Length scales

To get a better theoretical insight, we vary the length of our system, while keeping a fixed ratio between length and penetration depth of the laser, i.e., $\lambda L=$const. Thus we avoid the region of generation to become relatively larger in a smaller sample, so in the major part of the sample we always have transport of the carriers. Furthermore, we change the k_z dependence of (8) to

$$g_1'(k_z,z)=g_0'\delta(k_L^2-k_z^2)e^{-\lambda z}\ , \tag{14}$$

i.e., a generation rate, which is still symmetric in k_z and $-k_z$ and does not directly generate a total momentum. In this case, the ballistic transport can easily be recognized from the delta peaks in the distribution function at $\pm k_L$, and, at the same time, the singular behavior encountered for model (8) is avoided.

Figure 5(a) shows the density profiles for three different sample lengths L, 1, 5, and 20 μm. The penetration depth is always taken to be $\frac{1}{20}L$. Although the carriers are generated near $z=0$, in the short samples the maximum of the density can occur quite near the surface at $z=L$. In this case average velocities of the order of 10^6 cm/s are possible [Fig. 5(b)]. Increasing the excess energy up to the optical phonon energy and lowering the lattice temperature, we lower the transit time of a carrier through the sample and increase the scattering time. Figures 6(a) and 6(b) show the density and average velocity profiles for this case. The density in the 1-μm sample has almost no space dependence, in accordance with the analytical solution (12). This leads to the conjecture that the transport is to a large extent ballistic. Outside the generation region (i.e., neglecting $e^{-\lambda z}$ and $e^{-\lambda L}$), the analytical average velocity for ballistic transport with the generation model (14) is with (13)

$$\langle v\rangle=\frac{j}{n}=\frac{\hbar k_L}{m^*}\frac{1-R_L}{1+R_L}\ . \tag{15}$$

The average velocity does not depend on the reflection

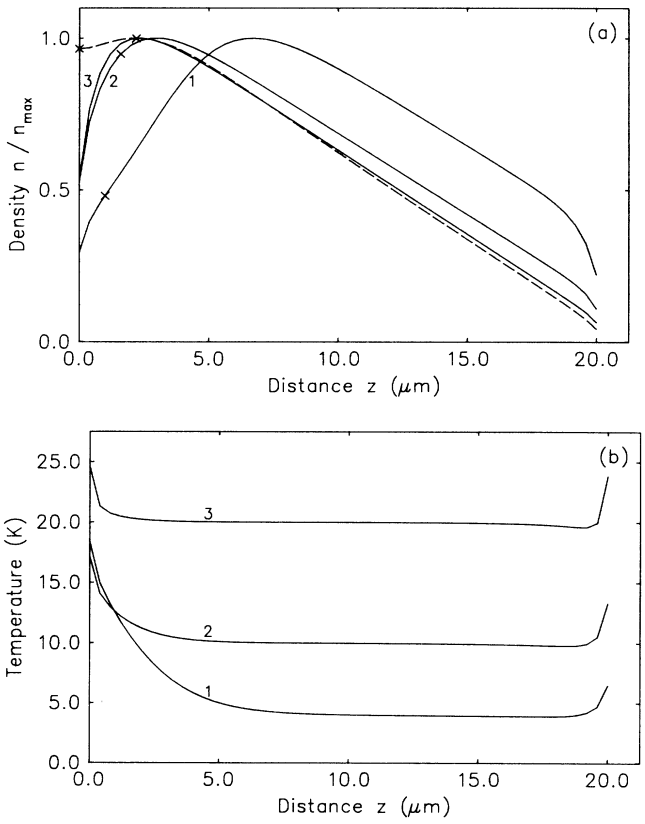

FIG. 4. (a) Density and (b) temperature profiles at $E_{\rm exc}=8$ meV and $R=0.5$ for lattice temperatures (1) 4 K, (2) 10 K, (3) 20 K. Dashed line: density profile for $R_0=1$, $R_L=0$, $T_L=10$ K, $E_{\rm exc}=28$ meV. For the position of the crosses see Fig. 3.

coefficient R_0 because this surface effectively modifies only the generation rate. The 1-μm sample nearly reaches this value, which is 7.3×10^6 cm/s for our parameters. But even in the 20-μm sample $\langle v \rangle$ is still larger than 10^6 cm/s. Figure 7 shows the distribution function $f(v_z,z)$ with fixed $z=0.6$ L and $v_z=\hbar k_z/m^*$ for the six cases as in Figs. 5 and 6. For the lower excess energy [Figs. 7(a)—7(c)] the shape of the distribution function is always approximately Maxwellian, only in the 1-μm sample the ballistic peaks appear. In the 5-μm sample a small structure at v_L is reminiscent of the generation process, whereas in the 20-μm sample the distribution function has relaxed towards a Maxwellian with lattice temperature 10 K. For the higher excess energies the distribution functions look quite different. Indeed, in the 1-μm sample the transport is mainly ballistic, most carriers are in the delta peaks. The 5-μm sample shows an intermediate type (like the 1-μm sample with the lower excitation), while the 20-μm sample contains practically no ballistic carriers. Comparing Figs. 7(c) and 7(f), we see that electron-phonon coupling has not been very effective, since the equilibrium distribution function for 4 K should be even narrower than that in Fig. 7(c). This fact together with the high average velocity [Fig. 6(b)] demonstrates, that we have a drift-dominated motion.

IV. SUMMARY

We have demonstrated that carrier kinetics sensitively depends on the injection and surface model. Though the resulting flow pattern can be mapped into a hydrodynamic description in terms of diffusive and drift contributions, a satisfying physical interpretation is possible only within the more detailed kinetic model.

In the case of strong temperature gradients reverse diffusion is possible, leading to a density profile with maximum $n_{\max}$ inside the sample even without surface recombination. This maximum can be quite far from the surface, where the carriers are generated. The corresponding spatial region should dominate the luminescence, and thus explain why in optical measurements the spectra can be fit by a single data set $(n_{\max},T,v_d)$.

We have shown, that under suitable conditions the surface can act as a source of net momentum due to reflection and recombination. The physical origin of drift in the absence of external forces has thus been clarified for the first time. According to the time scale, or for given parameters as excess energy, lattice temperature, and boundary conditions, according to a corresponding length-scale, different transport types are possible. On the shortest time scale transport is ballistic, each individual momentum being conserved. Thus, the process is strongly

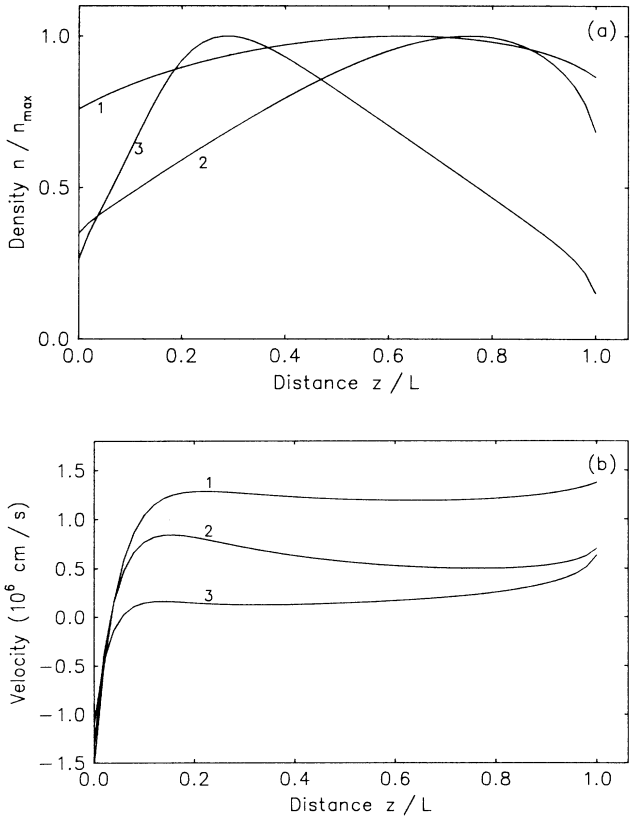

FIG. 5. (a) Density and (b) average velocity profiles at $R=0.5$, $\lambda L=20$, $E_{\rm exc}=8$ meV, $T_L=10$ K for (1) 1 μm, (2) 5 μm, (3) 20 μm length. The generation rate is according to Eq. (14).

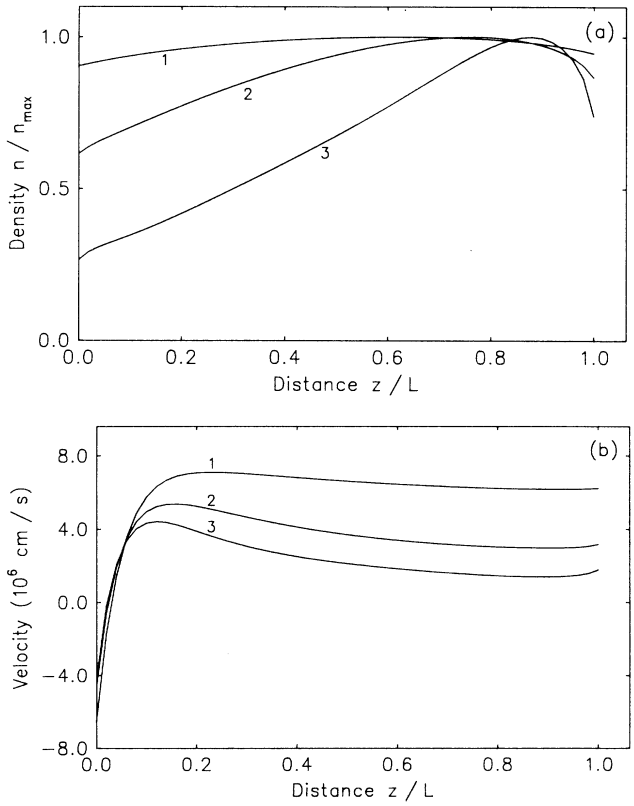

FIG. 6. (a) Density and (b) average velocity profiles at $R=0.5$, $\lambda L=20$, $E_{\rm exc}=60$ meV, $T_L=4$ K for (1) 1 μm, (2) 5 μm, (3) 20 μm length. The generation rate is according to Eq. (14).

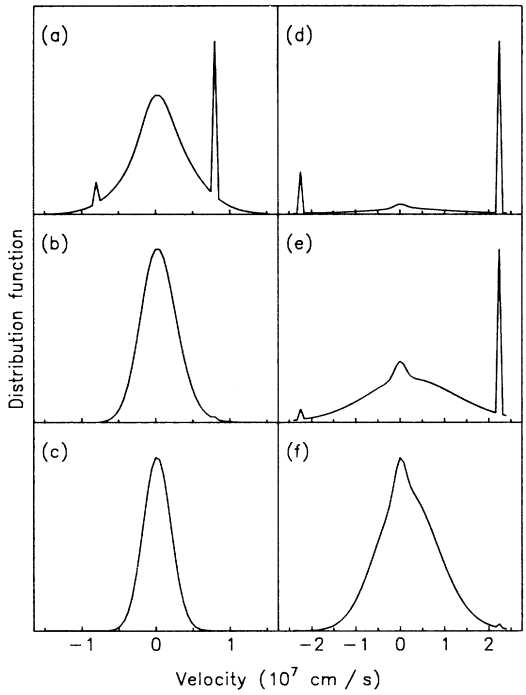

FIG. 7. Distribution functions $f(v_z,z)$ at fixed $z=0.6$ L. (a), (b), and (c) are for the parameters (1) , (2), and (3) of Fig. 5; (d), (e), and (f) for the parameters (1), (2), and (3) of Fig. 6, respectively.

non-Markovian, it depends on the details of carrier injection. On longer time scales electron-electron scattering is the dominant process, leaving the total momentum of the carrier distribution conserved, but thermalizing the carriers towards a displaced and heated Maxwellian. Finally, when the time scale becomes longer than the electron-phonon relaxation time, the net momentum relaxes towards zero and only spatial gradients can lead to a motion, the transport is of the usual diffusive type.

The average velocity, which may range from $\approx 0.1 v_s$ up to $\approx 10 v_s$ has been found to depend on much more experimental details than expected and specified so far. It is therefore not surprising to find seemingly contradictory answers in the measurements published up to now. Our investigations thus partly resolve long-standing controversies about electronic transport in semiconductors.

Our present approach has been based on several approximations. An extended version should include details of the band structure, quantum-statistical modifications, and nonequilibrium within the phonon system. We expect that these extensions would not qualitatively change our present results. The most fundamental remaining issue is the analysis of the phonon wind. In principle, this problem is very close to the electronic-drift problem. Surprisingly enough, the phonon-drift has enjoyed an almost general acceptance, despite the fact that, so far, little is known about its origin: The corresponding kinetic analysis including the influence of the surface is still lacking.

[1]T. Ytrehus, in *Kinetic Theories and the Boltzmann Equation*, edited by C. Cercignani (Springer, Berlin, 1984), p. 221.
[2]H. Neunzert, in *Kinetic Theories and the Boltzmann Equation*, edited by C. Cercignani (Springer, Berlin, 1984), p. 60.
[3]S. A. El Wakil, E. A. Saad, and A. A. Hendi, J. Phys. D **18**, 765 (1985).
[4]A. Forchel, B. Laurich, H. Hillmer, G. Tränkle, and M. Pilkuhn, J. Lumin. **30**, 67 (1985).
[5]M. A. Tamor, M. Greenstein, and J. P. Wolfe, Phys. Rev. B **27**, 7353 (1983).
[6]J. Doehler, J. C. V. Mattos, and J. M. Worlock, Phys. Rev. Lett. **38**, 726 (1977).
[7]A. Forchel, H. Schweizer, B. Laurich, G. Tränkle, and G. Mahler, in *Proceedings of the Materials Research Society*, edited by J. C. Fan and N. M. Johnson (North-Holland, New York, 1984), Vol. 23.
[8]A. Forchel, H. Schweizer, and G. Mahler, Phys. Rev. Lett. **51**, 501 (1983).
[9]H. Schweizer and E. Zielinski, J. Lumin. **30**, 37 (1985).
[10]H. Nather and L. G. Quagliano, J. Lumin. **30**, 50 (1985).
[11]J. P. Wolfe, J. Lumin. **30**, 82 (1985).
[12]F. M. Steranka and J. P. Wolfe, Phys. Rev. Lett. **53**, 2181 (1983).
[13]V. S. Bagaev, L. V. Keldysh, N. N. Sibel'din, and V. A. Tsvetkov, Zh. Eksp. Teor. Fiz. **70**, 702 (1976) [Sov. Phys.—JETP **43**, 362 (1976)].
[14]G. Mahler, G. Maier, A. Forchel, B. Laurich, H. Sanwald, and W. Schmid, Phys. Rev. Lett. **47**, 1855 (1981).
[15]G. Mahler and A. Fourikis, J. Lumin. **30**, 18 (1985).
[16]S. A. Trugman and A. J. Taylor, Phys. Rev. B **33**, 5575 (1986).
[17]E. M. Conwell, *High Field Transport in Semiconductors*, Suppl. 9 of *Solid State Physics* (Academic, New York, 1967).
[18]C. Jacoboni and L. Reggiani, Rev. Mod. Phys. **55**, 645 (1983).
[19]W. Fawcett, in *Electrons in Crystalline Solids*, edited by A. Salam (IAEA, Vienna, 1973), p. 531.
[20]H. U. Baranger and J. W. Wilkins, Phys. Rev. B **30**, 7349 (1984).
[21]K. Seeger, *Semiconductor Physics* (Springer, Vienna, 1973), p. 425.
[22]G. Mahler and A. Forchel, Helv. Phys. Acta **56**, 875 (1983).
[23]R. Castagné, Physica **134B**, 55 (1985).